How chemistry controls electron localization in $3d^1$ perovskites

O.K. Andersen and J. Nuss; E. Pavarini (INFM Pavia and MPI-FKF);
S. Biermann and A. Georges (Ecole Polytechnique Palaiseau);
A. Poteryaev and A.I. Lichtenstein (NSRIM Nijmegen)

Transition metal perovskites have been studied for decades because of their unusual electronic and magnetic properties arising from narrow 3*d* bands and strong Coulomb correlations. The $3d^1$ perovskites are particularly interesting since despite the lack of multiplet effects similar materials have very different electronic properties: strontium and calcium vanadate are correlated metals with mass-enhancements of respectively 2.7 and 3.6, while lanthanum and yttrium titanate are Mott insulators with gaps of respectively 0.2 and 1 eV.

Associated with the increasing electron localization along this series is a structural $GdFeO_3$-type distortion (Fig. 1 top): Whereas $SrVO_3$ is cubic, the corner-sharing BO_3 octahedra of the other perovskites are tilted and rotated in such a way that there are 4 equivalent octahedra per primitive cell. The reason often given for the progression of this distortion is that the size of the A cation relatively to that of the BO_3 octahedron shrinks along the series, i.e., that $r(Sr^{2+}) \sim r(La^{3+}) > r(Ca^{2+}) \sim r(Y^{3+})$, while $r(V^{5+}) < r(Ti^{3+})$.

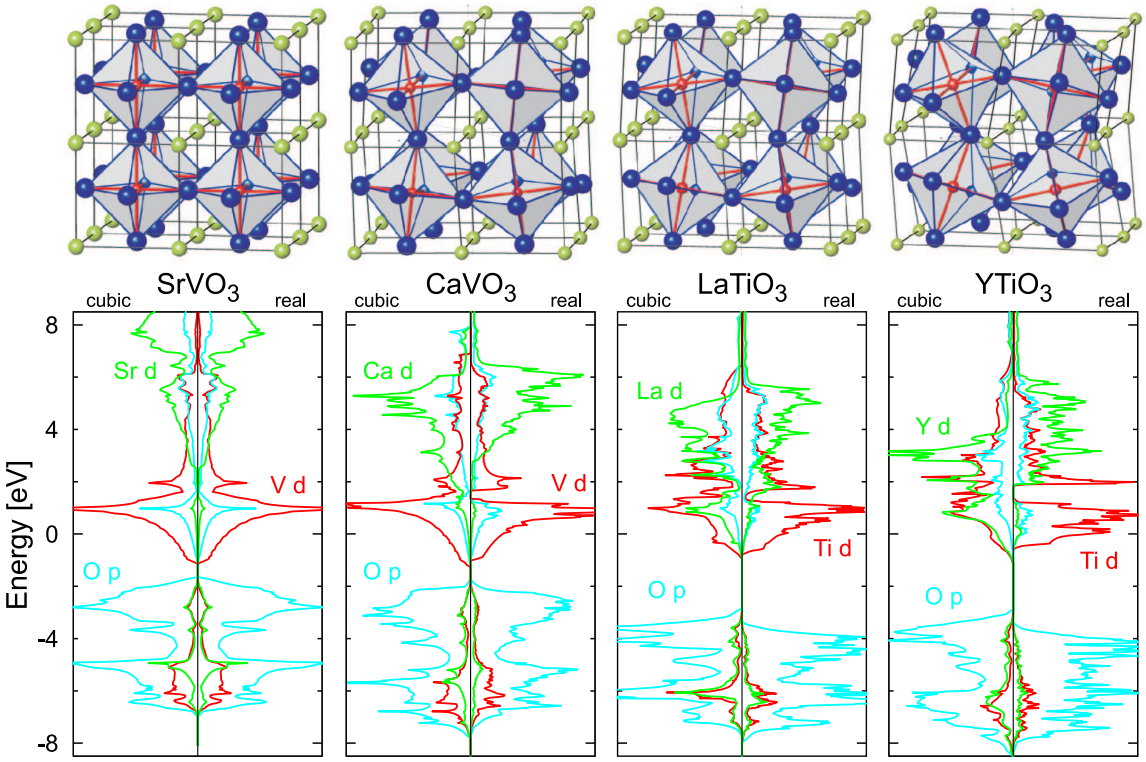

FIG. 1. Top: Structures of the $3d^1$ perovskites, A(green) B(red) O_3(blue). In a global, cubic *xyz*-system directed approximately along the BO bonds, the orthorhombic translations are $a = (1,\text{-}1,0)\,(1+\alpha)$, $b = (1,1,0)\,(1+\beta)$, and $c = (0,0,2)\,(1+\gamma)$, with α, β, γ small. In the *Pbnm* symmetry, the *ab*-plane through A is a mirror $(z \leftrightarrow -z)$, and so is the *bc*-plane through B $(x \leftrightarrow y)$ when combined with the translation $(b-a)/2$. The $GdFeO_3$-type distortion tilts the corner-sharing octahedra around the *b*-axis (by 0, 9, 12, and 20°) and rotates them around the *c*-axis (by 0, 7, 9, and 13°) as we progress from cubic $SrVO_3$ via $CaVO_3$ and $LaTiO_3$ to $YTiO_3$. Bottom: LDA partial-wave-projected densities of states (DOS) calculated for the real structures (right-hand panels) and for hypothetical cubic structures with the same volume (left-hand panels). The blue, red, and green DOS are projected onto respectively all O *p*, all B *d*, and all A *d* partial waves. For the B *d* band, t_{2g} is below e_g whereas the opposite is true for the A *d* band in the cubic structure. The Fermi level is at zero energy.

In addition, local density approximation (LDA) band structures (Fig. 1 bottom) point to the role of covalency between the cation *d* states (green) and the oxygen 2*p* states (blue): In cubic $SrVO_3$ each Sr ion has 12 nearest oxygens at the face centers. The 3*d* band of Ca lies lower, and thereby closer to the oxygen 2*p* band than the 4*d* band of Sr, and it is therefore conceivable that a $GdFeO_3$-type distortion, which pulls some of the oxygen neighbors closer to the A ion and thereby

increases the covalency with those, is energetically more favorable in $CaVO_3$ than in $SrVO_3$. The figure shows the associated increase of the Ca $4d-$O $2p$ gap. Going now from the vanadates to the titanates, the A and B cations become first- rather than third-nearest neighbors in the periodic table, and the A *d* band therefore becomes nearly degenerate with the Ti 3*d* band, and more so for Y 4*d* than for La 5*d*. Here it is only the $GdFeO_3$ distortion which, through increase of the A $d-$O $2p$ covalency, pushes the A *d* band above the Fermi level. This, as well as the concomitant lowering of the O 2*p* band, is seen in the figure.

The B 3*d* band is split by covalency with the 2*p* orbitals on the O_6 octahedron into three $pd\pi$-coupled, low-lying t_{2g} bands and two $pd\sigma$-coupled, higher-lying e_g bands. Simplest theories for the electronic properties of the d^1 perovskites are therefore based on a Hubbard model with 3 *degenerate*, $\frac{1}{6}$-filled t_{2g} bands per B ion. For such a model, the metal-insulator transition occurs when the ratio of the on-site Coulomb repulsion to the one-electron bandwidth exceeds a critical value $U_c/W \approx 2$. The progressive localization of the electron along the series is therefore ascribed to a progressive reduction of the t_{2g} bandwidth due to the increased bending of the $pd\pi$ hopping paths (BOB bonds) and, as may be seen from Fig. 1, also to the increased theft of oxygen character by A orbitals. This may not be the full explanation of the Mott transition, however, because if the orbital degeneracy can be reduced, U_c/W will be reduced because there are more hopping processes in many-particle than in single-particle theory. Now, reduction of the orbital degeneracy requires a t_{2g} *level-splitting*, Δ, merely of size ZW, the bandwidth associated with quasiparticle excitations. Close to the Mott transition, $Z \sim 1-U_c/W$. Unlike in e_g-band perovskites such as the d^{3+x} manganites where large (10%) cooperative Jahn-Teller (JT) distortions of the octahedra indicate that the e_g degeneracy is reduced and the orbitals are spatially ordered, in the t_{2g}-band perovskites the octahedra are almost perfect. The t_{2g} orbitals have therefore often been assumed to be degenerate. If that is true, Khaliullin *et al.* predicted that quantum fluctuations will lead to an *orbital liquid* [Ulrich *et al.* in the Progress Report 2002, pp 47–51]. Moreover, an important experimental constraint on the nature of the orbital physics is the observation of an isotropic, small-gap spin-wave spectrum in both insulators. This is remarkable because $LaTiO_3$ is a 3-dimensional antiferromagnet with $T_N = 140$ K, a small moment ($0.45\,\mu_B$), and a recently discovered small JT distortion (3% stretching along *a*), while $YTiO_3$ is a ferromagnet with a low Curie temperature ($T_C = 30$ K), a good-sized moment ($0.8\,\mu_B$), and a JT distortion of different type (3% stretching along alternatively *x* and *y*).

We have calculated the electronic properties in the high-temperature ($T > T_{N,C}$) paramagnetic phases using a low-energy multiband Hubbard Hamiltonian,

$$H = H^{\rm LDA} + \frac{1}{2}\sum\nolimits'_{{\rm imm}'\sigma\sigma'} U_{{\rm imm}'}\,\hat{n}_{{\rm im}\sigma}\,\hat{n}_{{\rm im}'\sigma'} - {\rm d.c.}, \quad (1)$$

whose one-electron part is given by the local approximation to density-functional theory (LDA) and whose on-site (*i*) Coulomb interactions are included for a subspace of localized orbitals *(im)*. The LDA provides a parameter-free account of the materials dependence, i.e., the chemistry. Recently it has become possible to solve this Hamiltonian in the dynamical mean-field approximation (DMFT), as is described in the contribution by Held *et al.* (see pp 50). In previous LDA+DMFT implementations it was assumed that the on-site block of the single-particle Green function is diagonal in the space of the correlated orbitals which were taken as orthonormal LMTOs, approximated by truncated and renormalized partial waves. These approximations are good for cubic t_{2g} systems such as $SrVO_3$, but they deteriorate with the degree of distortion. We have therefore used localized *Wannier functions* and included the non-diagonal part of the on-site self-energy in the DMFT.

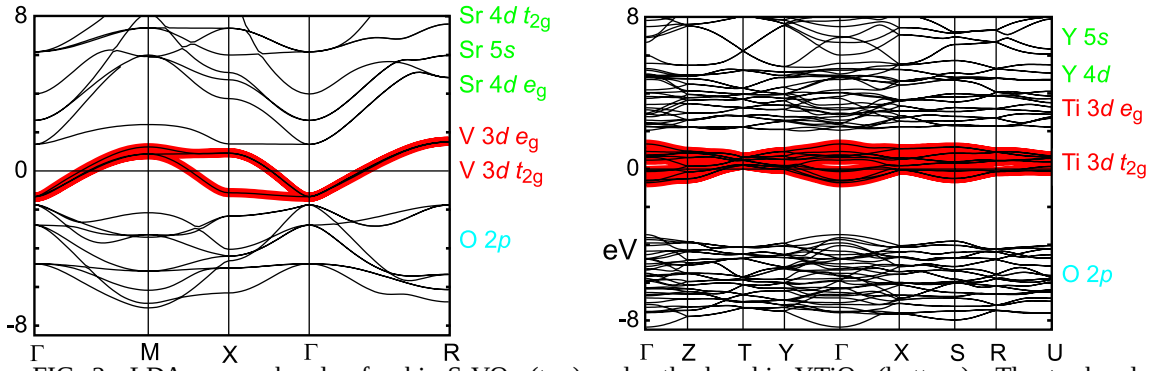

FIG. 2. LDA energy bands of cubic $SrVO_3$ (top) and orthorhombic $YTiO_3$ (bottom). The t_{2g} bands obtained with the full (black) and downfolded (red) NMTO basis sets are identical.

For an isolated set of bands, a set of Wannier functions constitutes a *complete*, orthonormal set of orbitals with *one* orbital per band (Fig. 2). For the d^1 perovskites we take the correlated orbitals to be three localized B t_{2g} Wannier orbitals, and in $H^{\rm LDA}$ we neglect the degrees of freedom from all other bands. In order to be complete, such a Wannier orbital must have a tail with e.g., O *p* and A *d* characters. Our Wannier orbitals are symmetrically orthonormalized $N^{\rm th}$-order muffin-tin orbitals (NMTOs), which have all partial waves other than B *xy*, *yz*, and *zx* downfolded. For the on-site Coulomb interactions we use the common assumption that, as in the isotropic case, they can be expressed in terms of two parameters, U and J. The former we take to be 5 eV for all four perovskites, and the latter has been calculated to be 0.68 eV for the vanadates and 0.64 eV for the titanates. The self-energy can now be obtained from the solution of an effective Anderson impurity model which involves only 3 correlated orbitals. All components of the self-energy matrix $\Sigma_{\rm mm'}(\omega)$ between different Wannier functions on a given B-site are taken into account. From this 3×3 matrix, by use of the symmetry (Fig. 1), we construct a 12×12 block-diagonal self-energy matrix. This is then used together with $H^{\rm LDA}(\mathbf{k})$ to obtain the Green function at a given $\mathbf{k}$-point. Fourier transformation over the entire Brillouin zone yields the local Green function associated with a primitive cell and its 3×3 on-site block is used in the DMFT self-consistency condition in the usual manner. The 3-orbital impurity problem is solved by a quantum Monte Carlo scheme which is accurate at high temperature.

Figure 3 displays the LDA on-site DOS matrix, $\rm N_{mm'}(\varepsilon)$, in that representation of the t_{2g} Wannier orbitals which diagonalizes the on-site term of $H^{\rm LDA}$, i.e., the ligand and crystal-field term. The t_{2g} band of cubic $SrVO_3$ consists of three degenerate subbands, and since the *xy*,*yz*, and *zx* orbitals hardly interact, each subband is nearly

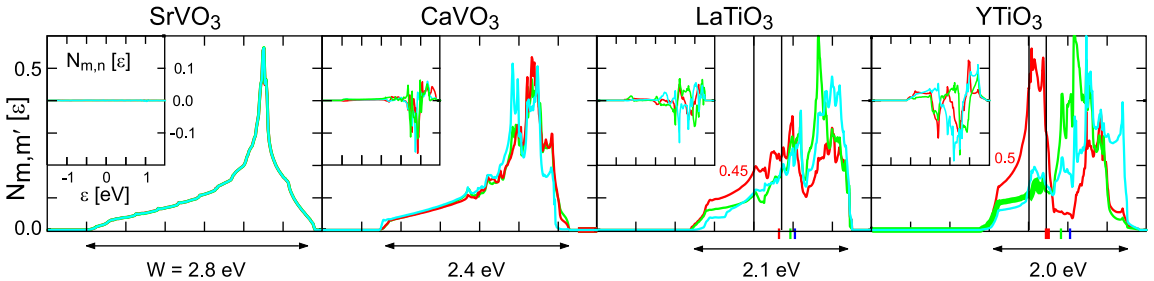

FIG. 3. LDA on-site DOS matrix, $N_{\rm mm'}(\varepsilon)$, in the representation of t_{2g} Wannier orbitals which diagonalizes the on-site term of $H^{\rm LDA}$. The insets give the off-diagonal elements. In the vanadates, the eigenfunctions are *xy*, *yz*, and *zx*. In $SrVO_3$, these orbitals are degenerate, but in $CaVO_3$, the energy of the *xy* orbital (blue) is $\Delta = 0.08$ eV below that of the two other orbitals. In the titanates there are three singly-degenerate levels with the lowest (red) being 0.14 eV below the middle in $LaTiO_3$ and 0.20 eV in $YTiO_3$. The lowest-energy eigenfunctions are shown in Fig. 5.

2-dimensional and gives rise to a nearly logarithmic DOS peak. Going to $CaVO_3$, the bandwidth is reduced from 2.8 to 2.4 eV for the reasons mentioned before, and the energy of the *xy* orbital (the center of gravity of $N_{xy,xy}$) is lowered by 0.08 eV compared to that of the degenerate *xz* and *yz* orbitals. Going from the vanadates to the titanates, the increased misalignment and loss of oxygen character further reduce the bandwidths to 2.1 and 2.0 eV. Moreover, the *xy*, *yz*, and *zx* Wannier orbitals mix and the levels split with the middle (highest) being 0.14 (0.20) eV above the lowest in $LaTiO_3$, and 0.20 (0.33) eV in $YTiO_3$. Finally, there are strong off-diagonal elements of the DOS matrix even in the eigenrepresentation of H_{on}^{LDA}. In $YTiO_3$, the diagonal DOS element for the orbital with the lowest energy exhibits a pseudogap. Despite the strong increase of the level splittings, Δ, they remain an order of magnitude smaller than the t_{2g} bandwidths, and also smaller than the subband-widths.

As a consequence, the eigenfunction for the lowest level is occupied by merely 0.45 electron in $LaTiO_3$ and 0.50 in $YTiO_3$. Nevertheless, the splittings are large compared with the spin-orbit splitting (20 meV) and kT, and they are not caused by the JT distortions, as we have verified by turning them off in the calculations.

By performing LDA+DMFT calculations for several values of U between 3 and 6 eV, we found that the critical ratio $(U-2J)_c/W$ decreases from 2 to 1.4 when going along the series. This is consistent with an increasing Δ, and it indicates that the Mott transition is driven as much by the decrease of effective degeneracy (from 3 to almost 1) as by the reduction of bandwidth. As shown in Fig. 4, the main features of the experimental photoemission spectra for all four materials, as well as the correct values of the mass enhancements for the metals and the Mott-Hubbard gap for the insulators, are reproduced by taking U constant ≈ 5 eV. This is satisfying, because U is expected to be similar for vanadates and titanates. Despite very similar bandwidths for $LaTiO_3$ and $YTiO_3$, the gaps are very different, 0.2 and 1 eV. This is consistent with our findings that the t_{2g} level splittings are larger and $(U-2J)_c/W$ smaller in $YTiO_3$ than in $LaTiO_3$. Diagonalization of the matrix of occupation numbers reveals that for the titanates *one orbital per site is nearly full* and that this orbital is nearly identical with the one we obtained from the LDA as having the lowest energy. The Coulomb correlations increase its occupation from 0.45 to 0.88 in $LaTiO_3$ and from 0.50 to 0.96 in $YTiO_3$. This orbital polarization increases around the metal-insulator transition and becomes complete thereafter. In the vanadates, each orbital is approximately 1/3 occupied for all U in the range from 0 to 6 eV. The nearly complete orbital polarization in the titanates indicates that correlation effects in the paramagnetic Mott insulating state considerably decrease orbital fluctuations, and makes it unlikely that $YTiO_3$ is a realization of an orbital liquid. In $LaTiO_3$ some orbital fluctuations are still active, although quite weak. Whereas the localization is caused by Coulomb correlations, the chemistry (LDA) selects the orbital (Fig. 5). For illustration of the orbital order, we have placed this orbital on each of the 4 Ti-sites. Although $LaTiO_3$ and $YTiO_3$ have the same space group, their orbital orders look different.

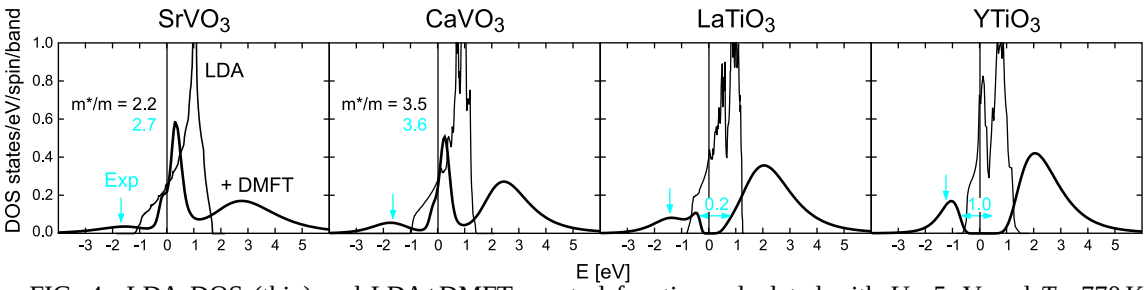

FIG. 4. LDA DOS (thin) and LDA+DMFT spectral function calculated with $U = 5$ eV and $T = 770$ K (thick). Results from optical conductivity and photoemission measurements are indicated in blue.

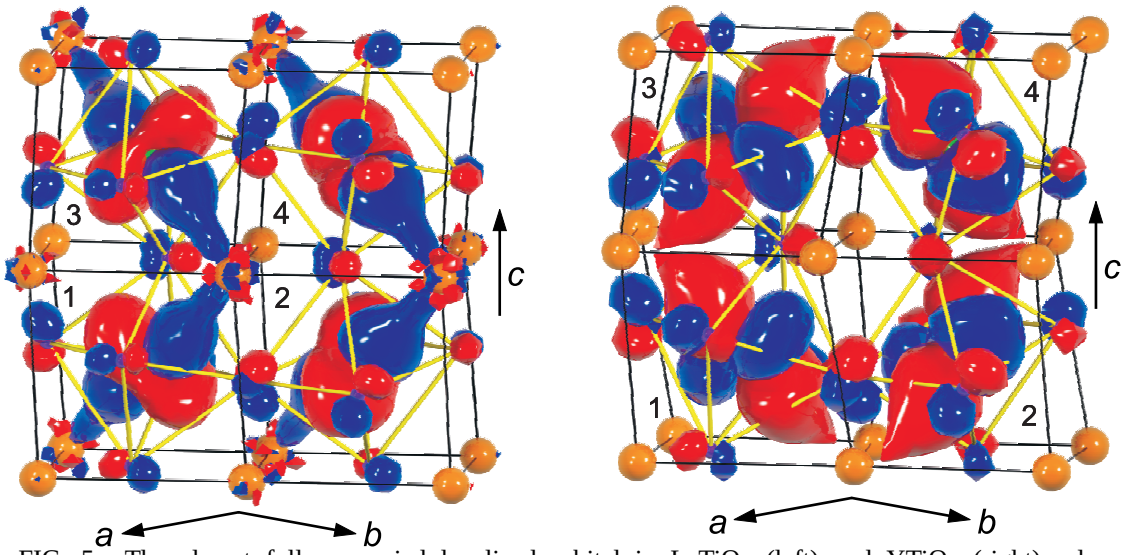

FIG. 5. The almost fully occupied localized orbital in $LaTiO_3$ (left) and $YTiO_3$ (right), placed on each of the 4 Ti-sites to exhibit the orbital order. On site 1, this orbital is the linear combination $0.586|xy\rangle + 0.275|xz\rangle + 0.762|yz\rangle$ of the Ti t_{2g} Wannier functions in $LaTiO_3$ and $0.622|xy\rangle - 0.029|xz\rangle + 0.782|yz\rangle$ in $YTiO_3$. Blue and red indicate respectively positive and negative values. A relatively low numerical value of the contour has been used in order to bring out covalency effects.

This difference reflects the extent to which the orbital has the *bc*-plane through Ti as a mirror, and is only quantitative. What causes this particular Ti t_{2g} orbital to have the lowest energy is *cation covalency* and crystal-field effects: the positive (blue) lobes have bonding $3z^2_{111} - 1 = (xy + xz + yz)/\sqrt{3}$ character on the *nearest* A cations and the negative (red) lobes have bonding *xy* character on the next-nearest A cations which continues in bonding $(x-y)/\sqrt{2}$ character on the oxygen closest to that cation. The former type of AB covalency dominates in $LaTiO_3$, while the latter type of ABO covalency dominates in $YTiO_3$, where the shortest YO bond is merely 10% longer than the TiO bond. The LDA pseudogaps as well as the level splittings are thus caused by the A *d* character not used to drive the $GdFeO_3$ distortion, but left behind in the Ti t_{2g} band (Fig. 1).

The different JT distortions of the oxygen square in $LaTiO_3$ and $YTiO_3$ are a reaction to, rather than the cause of the difference in the orbital orders. The difference in the orbital orders is reflected in the hopping integrals between nearest neighbors: $t_x = t_y = 99\,(38)$ meV and $t_z = 105\,(48)$ meV for $LaTiO_3$ ($YTiO_3$). These hoppings are fairly isotropic and twice larger in $LaTiO_3$ than in $YTiO_3$. Moreover, the hoppings to the two excited orbitals are stronger in $YTiO_3$ than in $LaTiO_3$. All of this is consistent with $LaTiO_3$ being 3-dimensional anti- and $YTiO_3$ ferromagnetic at low temperature, and it warrants detailed future calculations of the spin-wave spectra.

We have thus seen that the B t_{2g} degeneracy *is lifted* at the classical level. This is not due to the small JT distortions via OB *pd*π-coupling, but to the $GdFeO_3$-type distortion. This distortion is driven by the increasing OA *pd*σ-covalency, and it primarily pulls 4 of the 12 oxygens neighboring a given A cation closer to it. Moreover, 2 to 4 of the 8 A cations neighboring a given transition metal ion (B) are pulled closer. The B t_{2g} orbitals couple to the OA distortion via oxygen (BOA *dp*π–*pd*σ), and they couple directly (AB *dd*σ) to the AB distortion.

In conclusion, we have extended the LDA+DMFT approach to the non-cubic case using ab initio downfolding in order to obtain a low-energy Wannier Hamiltonian. Applying this method to the Mott transition in $3d^1$ perovskites, we have explained the photoemission spectra and the values of the Mott gap without adjustable parameters, except a single value of *U*. The Mott transition is driven by correlation effects and $GdFeO_3$-type distortion through reduction, not only of bandwidth, but also of effective orbital degeneracy. Correlation effects and cation covalency suppress orbital fluctuations in the high-temperature paramagnetic insulating phase of $LaTiO_3$ and $YTiO_3$.